

Lehigh University Lehigh Preserve

Fritz Laboratory Reports

Civil and Environmental Engineering

1970

Shear in beam-to-column connections, September 1970 (71-21)

David J. Fielding

Joseph S. Huang

Follow this and additional works at: <http://preserve.lehigh.edu/engr-civil-environmental-fritz-lab-reports>

Recommended Citation

Fielding, David J. and Huang, Joseph S., "Shear in beam-to-column connections, September 1970 (71-21)" (1970). *Fritz Laboratory Reports*. Paper 298.
<http://preserve.lehigh.edu/engr-civil-environmental-fritz-lab-reports/298>

This Technical Report is brought to you for free and open access by the Civil and Environmental Engineering at Lehigh Preserve. It has been accepted for inclusion in Fritz Laboratory Reports by an authorized administrator of Lehigh Preserve. For more information, please contact preserve@lehigh.edu.

F.L. 333.9

FRITZ LABORATORY REPRINT No. 71-21

SHEAR IN STEEL BEAM-TO-COLUMN CONNECTIONS

by
David J. Fielding
Joseph S. Huang

Reprinted from THE WELDING JOURNAL, Vol. 50, July 1971,
published by the American Welding Society, Miami, Florida

Shear in Steel Beam-to-Column Connections

The current AISC design formula is shown to be conservative by theoretical analysis and tests of a full size beam-to-column connection subjected to moment, shear and high axial loads

BY D. J. FIELDING AND J. S. HUANG

ABSTRACT.—The condition of high shear stress in rigid frame connections and the effect of high axial force is investigated. A yield condition is derived and verified by a test. After yielding in the test specimen, stable joint deformation was observed under monotonic loading and the connection carried 2.75 times what is considered to be the yield strength in shear. The current AISC design formula is shown to be conservative.

Introduction

It is frequent practice in structural frame analysis to consider that the connections are the intersections of beam and column centerlines and that these junctions are rigid. According to this assumption there is no relative change in angle of rotation between a beam centerline and a column centerline. Actually a real connection should be considered as a structural member with finite dimensions and loading.

Figure 1 shows an interior structural connection with an antisymmetrical loading as would be caused by wind or earthquake. The axial forces in the beams are usually negligible. A similar loading occurs on an exterior connec-

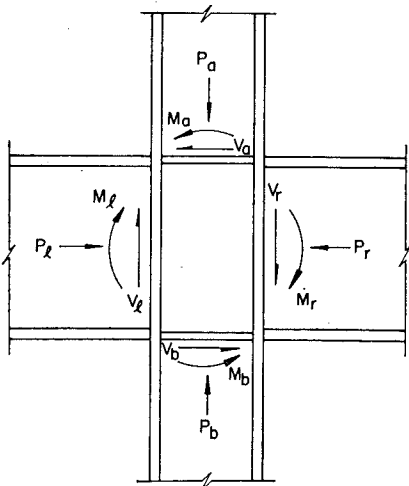


Fig. 1—Interior beam-to-column connection

tion under wind or gravity types of loading. If the moment M in Fig. 2 is replaced by the forces T where

$$T = \frac{M}{d_b} \quad (1)$$

and d_b is the beam depth, then the high column-web shear force becomes apparent. The design of the connection shear stiffeners is based on this large shear force^{1,2} by limiting the shear stress τ to the value $\sigma_y/\sqrt{3}$ according to the Von Mises yield criterion. This is usually written as

$$\tau = \frac{T}{A_w} \quad (2)$$

where A_w is the area of the column web in the connection. If no shear stiffening is present in the column web then

$$A_w = d_c w \quad (3)$$

in which d_c is the column depth and w is the thickness of the web in the connection. If shear stiffening is present, an effective web area should be used. Combining eqs (1), (2), and (3) gives the 1969 AISC design formula from the Commentary of the Specification, Sections 1.5.1.2 and 2.5

$$w \geq \frac{\sqrt{3} M}{\sigma_y d_b d_c} \quad (4)$$

Actually d_b and d_c should be distances between flange centroids. If this formula is used the column web within the connection will be prevented from yielding under the action of the beam moment M in Fig. 2. However, referring to Fig.

D. J. FIELDING and J. S. HUANG are with the Fritz Engineering Laboratory, Dept. of Civil Engineering, Lehigh University, Bethlehem, Pa.

The work described in this paper was carried out as part of an investigation sponsored jointly by the American Iron and Steel Institute and the Welding Research Council—publication of the paper was sponsored by the Structural Steel Committee of the Welding Research Council.

1, the design formula can be generalized to include the additional shear force from M_l for an interior connection and the reduction in shear force due to the column shear V_a to give²

$$w \geq \frac{\sqrt{3}}{\sigma_y d_c} \left(\frac{M_r}{d_b} + \frac{M_l}{d_b} - V_a \right) \quad (5)$$

This formula dictates shear stiffening for a connection based on a more realistic value of shear force but independently of the column loading P_a in Fig. 1. If P_a is at the ultimate column load, eqs (4) and (5) still imply the same column web shear capacity as if P_a were not present. This inconsistency along with observed column web shear deformation in a frame test³ prompted the current study of the effect of axial load on connection design.

In 1966 a series of seven pilot tests was begun on simulated exterior connections. Two of the seven tests were designed so that the column web within the connection would yield in shear; however, in all seven tests, failure

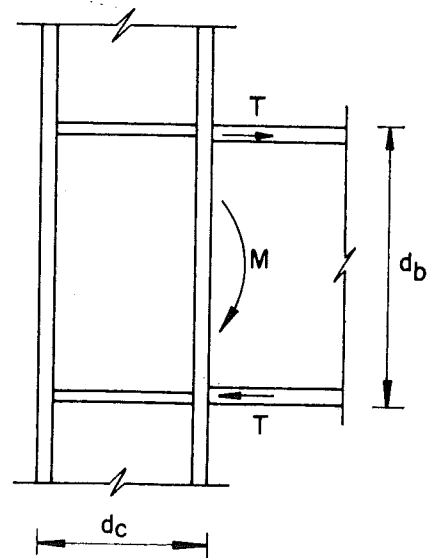


Fig. 2—Exterior beam-to-column connection

occurred by the formation of plastic hinges outside the connection and at loads very much in excess of the predicted failure loads⁴. In the study it was concluded that connection shear deformations were larger for higher axial load. At that point it was obvious that the shear capacity of an unstiffened connection should be based on an allowable story drift limit and not on some imaginary ultimate load expressed by bound solutions using plasticity limit theorems.⁴ A study of the elastic behavior of connections has been done,⁵ and a study of the inelastic behavior is underway at Lehigh University. The test of a beam and column assemblage reported herein is part of the latter investigation. The objective of the test was to study the influence of axial force on the behavior of beam-to-column connections that must also carry high shear from beam moment.

In order to attain the test objectives, requirements placed on the assemblage were:

1. That the connection be very low in shear resistance.
2. That the column web within the connection carry large axial force in addition to high shear force.

Theoretical Analysis

Assumptions

A beam-to-column connection can be

loaded as indicated in Fig. 1 in which there is a high moment gradient or shear within the connection. In Fig. 3 is shown an assemblage of a column and cantilever beam. The elastic column moment and shear diagrams are also indicated. The portion of the moment diagram within the connection is not actually known but can be assumed as a linear transition indicated by the dashed line. This assumption gives rise to the shear diagram in Fig. 3 indicating uniform shear throughout the column web. This is equivalent to saying that the beam moment M_r enters the connection as shear at the beam flange as indicated in Fig. 2. This is reasonable because most of the beam moment is carried in the flanges for wide-flange shapes.

Two points are important in this argument. First, the assumed force couple is statically equivalent to the real moment and, therefore, equilibrium is maintained at the connection. Second, the complexity of an exact solution of the stress distribution within the connection coupled with past observations of the pattern and effect of yielding warrants a simplified approach.

It is often implied that this connection shear force is carried by the column web as a uniform shear stress as in eq (2). Although an elastic solution⁵ using an Airy stress function shows

that the distribution is a parabolic variation from a constant stress at the edges, the error in assuming a uniform distribution is small. This is the same approximation that is made concerning the shear stress distribution in beam webs. In addition, the experimental results reported by Naka *et al.*⁵ show that the elastic shear stress distribution computed from strain gage data is more nearly uniform than parabolic. Therefore, the assumption of uniform shear stress in the connection panel is made.

In order to evaluate the behavior of the connection some reference loads must be calculated. Considering the structure in Fig. 3 there are four possible failure modes. First, M_r can reach the plastic moment for the beam before the column fails. Second, the plastic moment for the column can be reached at sufficient locations to cause a column mechanism. For the fixed-end column in Fig. 3 three plastic hinges are required;⁶ M_a , M_b , and M_L will reach the plastic moment first. A third failure mode could occur if the column web is thin, that is, shear buckling of the web. Normally the column web dimensions are such as to preclude shear buckling. If the column depth d_c , flange thickness t_f , and web thickness w (including doubler plate thickness) satisfy the ratio

$$\frac{d_c - 2t_f}{w} \leq 70 \quad (6)$$

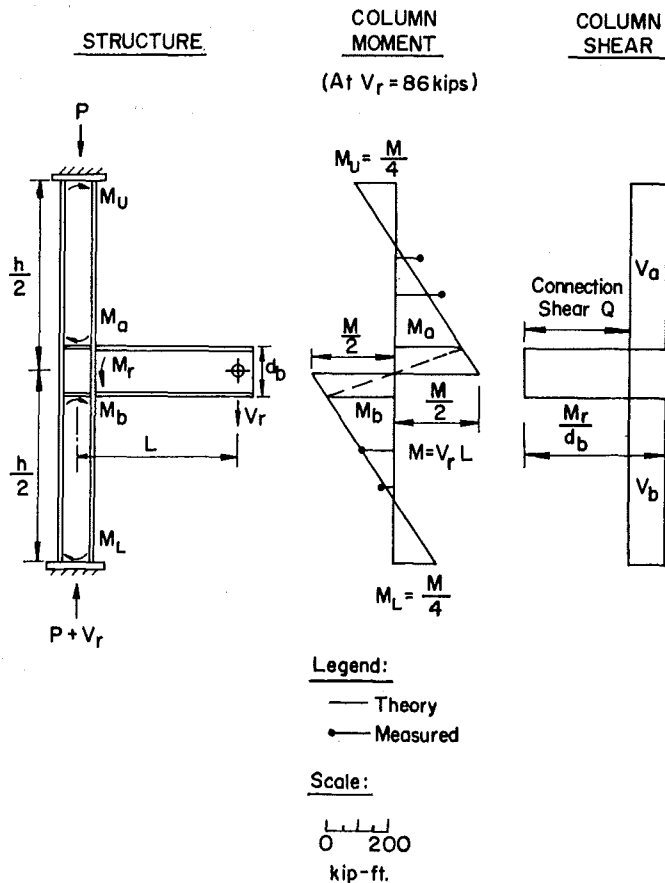


Fig. 3—Column moment and shear diagrams

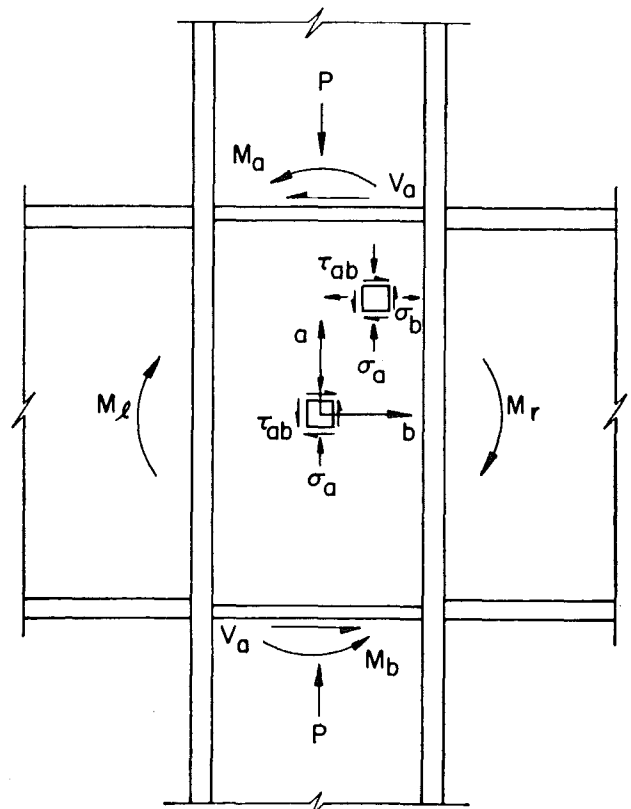


Fig. 4—Connection stress states

shear buckling will not be a problem.¹

The fourth failure mode is that of general yielding in the column web due to the high shear force that is present. This mode of failure is stable in nature—that is, there is no unloading. Although the web of a wide-flange beam is yielded due to shear, the beam will continue to carry additional load until shear deformation becomes excessive.² This same behavior was observed in the test of a corner connection⁸ in which the stiffness decreased substantially but with no instability. This fourth failure mode is the object of this study and, in the following analysis, is assumed to be critical.

Von Mises Yield Criterion

The Von Mises yield criterion or the maximum distortion energy theory of failure⁹ for biaxial stress state as exists in a joint panel is written:

$$\sigma_a^2 - \sigma_a\sigma_b + \sigma_b^2 + 3\tau_{ab}^2 = \sigma_y^2 \quad (7)$$

where a and b refer to the coordinate axes in Fig. 4. In one test,⁴ strain gages were applied on the column web within the connection and the principal stresses were calculated and recorded. From these data for a connection with no added shear stiffening it can be seen that the left hand side of eq (7) is approxi-

mately constant. This means that eq (7) can be solved for any single convenient point in the connection panel rather than at every point and that the connection panel yields throughout at a unique loading.

At the center of the connection in Fig. 4, σ_b can be taken as zero and σ_a can be taken as

$$\sigma_a = \frac{P}{A_c} = \left(\frac{P}{P_y}\right) \sigma_y \quad (8)$$

where A_c is the column area and $P_y = \sigma_y A_c$ is the yield load of the column. From previous discussion² the shear stress is written:

$$\tau_{ab} = \frac{1}{A_w} \left(\frac{M_r}{d_b} + \frac{M_l}{d_b} - V_a \right) \quad (9)$$

Substituting eq (8) into eq (7) gives:

$$\left(\frac{P}{P_y}\right)^2 + \frac{3\tau_{ab}^2}{\sigma_y^2} = 1 \quad (10)$$

This equation can be solved for $\tau_{ab} = \tau_y'$, a reduced yield stress in shear. When τ_{ab} in eq (9) is equal to τ_y' the entire column web will yield due to combined axial load and shear. Equating the right hand side of eq (9) to τ_y' , any of the interrelated moments and shear can be calculated as a limiting

value. Unlike eqs (4) and (5) currently used in design^{1,2} and which ignore axial force, eq (10) indicates that τ_{ab} must be zero when $P = P_y$ (column fully yielded by axial load).

The equations derived can be used to predict general yielding of a connection. Although such information is inadequate to predict ultimate capacity, it is useful in predicting the point at which inelastic action begins. This will be discussed again in light of experimental results.

Equations 9 and 10 can be combined to give an interaction equation similar to eq (5):

$$w \geq \frac{\sqrt{3} \left(\frac{M_r}{d_b} + \frac{M_l}{d_b} - V_a \right)}{\sigma_y d_c \sqrt{1 - \left(\frac{P}{P_y} \right)^2}} \quad (11)$$

This formula specifies the column web thickness required to prevent general yielding under the action of antisymmetrical beam moments M_r and M_l and column load P .

Conversely, eq (11) can be used to compute the moment M_r that will cause yielding of a column web with thickness w . All the moments and shears in eq (11) are related by the equations of static equilibrium.

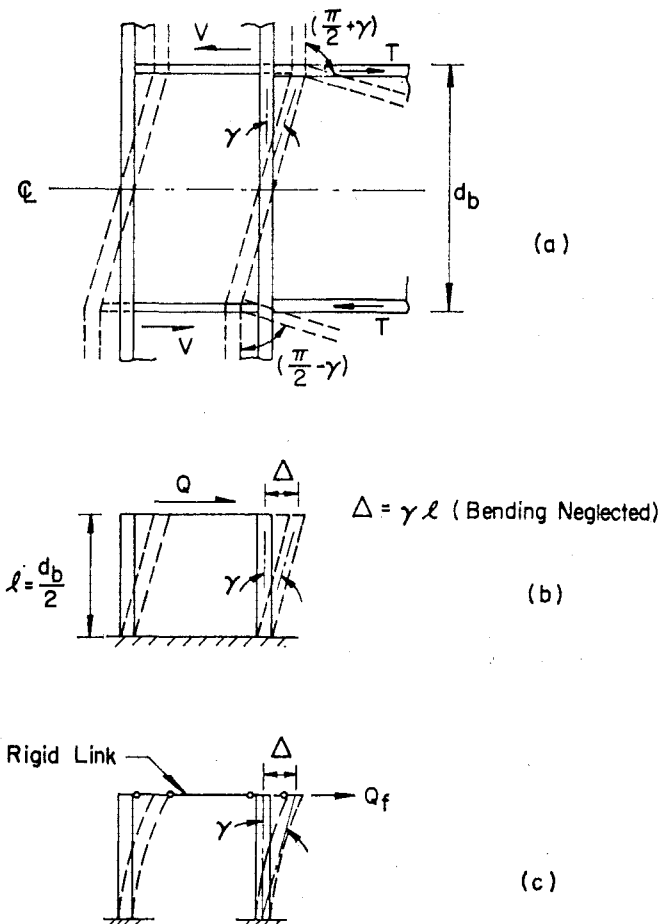


Fig. 5—Connection loading and equivalent cantilever

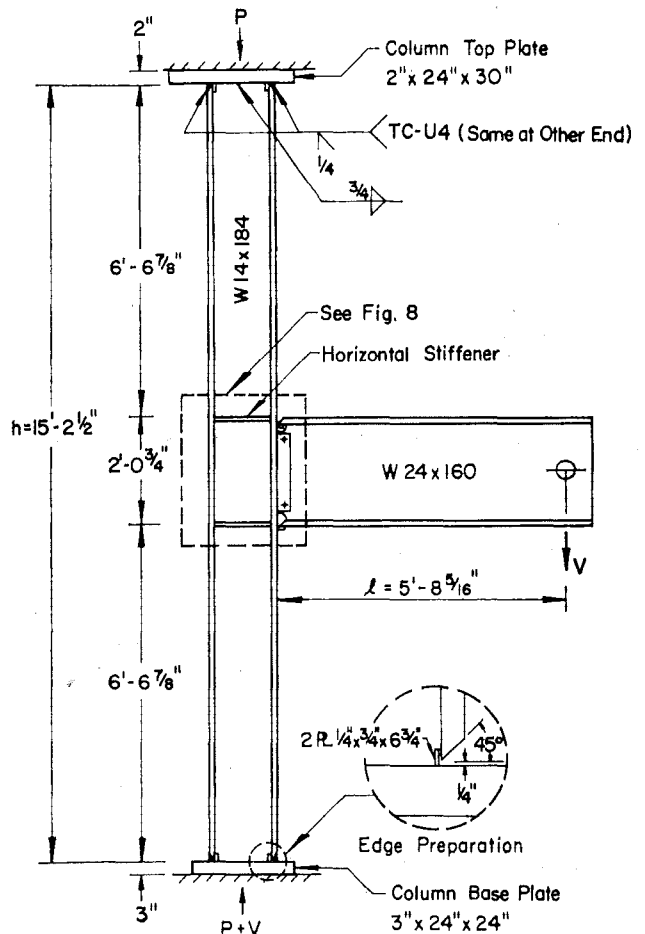


Fig. 6—Connection assemblage—B1

Elastic Connection Behavior

The shear force in the connection of Fig. 5(a) is:

$$Q = T - V \quad (12)$$

The shear stress τ is

$$\tau = \frac{Q}{A_w} \quad (13)$$

and, from $\tau = G\gamma$, the elastic shear deformation of the column web within the connection can be computed as:

$$\gamma = \frac{Q}{GA_w} \quad (14)$$

The bending deformation within the connection has been neglected but can be included as others did.⁸ The shear deformation γ from eq (14), measured in radians, will be the relative angle change from the right angle between the beam and column centerlines. This deformation is normally neglected in frame analysis. The angle γ is not a strain at a point but rather the gross average panel shear deformation.

It is apparent that the connection in Fig. 5(a) can be represented by the cantilever in Fig. 5(b) whose length is one-half the beam depth. Equations (13) and (14) are the same for the cantilever and the connection. The limit of elastic behavior will be at $\tau = \tau_y'$ when there is general yielding of the web in shear. At this point:

$$Q_y = \tau_y' A_w \quad (15)$$

and

$$\gamma_y' = \frac{\tau_y'}{G} \quad (16)$$

Post-Yield Behavior

The preceding equations predict general yielding of a connection panel. It is not necessarily true that the column flanges bounding the joint are also yielded. If they are elastic there will be some remaining elastic stiffness of the connection until these flanges too are fully yielded by the monotonic loading. This elastic stiffness can be computed from the model in Fig. 5(c) in which the flanges, connected by a rigid link, bend independently of the web.

$$\Delta = \frac{Q_f \ell^3}{3E(2I_f)} = \gamma \ell \quad (17)$$

where Q_f is the portion of Q carried by the flanges and I_f is the moment of inertia of each flange ($b_f \times t_f$).

$$I_f = \frac{1}{12} b_f t_f^3 \quad (18)$$

For this model, the interaction between the web and flanges after yielding has been neglected since it is assumed that the web will deform freely. This model is used only after the connection panel is yielded.

Of particular importance in computing connection deformation is the stiffness, or the ratio of shear force to shear strain, $\frac{Q}{\gamma}$. When the connection is elastic,

$$\frac{Q}{\gamma} = GA_w \quad (19)$$

This is obtained from eq (14) assuming that the flange contribution Q_f is negligible. When the column web yields, the elastic shear modulus G will become zero as evidenced by tests.¹⁰ However, the flange contribution from eq (17) gives:

$$\frac{Q_f}{\gamma} = \frac{24 EI_f}{d_b^2} \quad (20)$$

where ℓ has been taken as half the beam depth d_b .

The stiffness of the connection for an inelastic web is still based on the elastic modulus and section dimensions as long as the flanges have not fully yielded. This appears to be reasonable if one considers the large shear strains that are required before the connection panel can strain harden. It is not implied that strain-hardening does not occur locally but that the shear stiffness immediately after yielding of the column web is provided by the remaining elastic material in the column flanges. At larger strains eq (20) will not be reliable as the flanges too become yielded. However, at larger strains it is possible for the entire connection web to strain harden. This strain-hardening effect has not been included in this analysis nor has the limit of flange contribution in the inelastic range.

The limiting shear for this behavior must theoretically correspond to the formation of a plastic mechanism.² However, tests have indicated increased capacity due to the occurrence of strain-hardening in regions of moment gradient.¹¹

Description of Test

The single test described in this section was proposed to study the behavior of steel frame connections under antisymmetrical moment loading and axial loading.¹² Pilot tests⁴ indicated that axial load has some effect on yielding and deformation of connections and so special emphasis was placed on these factors.

Design of Assemblage

The assemblage shown in Fig. 6, designated *BI*, represents an exterior column and the left hand portion of a beam from a multistory frame. The particular beam and column sections were chosen with two objectives in mind. First, the loads that cause failure within the connection web panel were to be

much lower than the loads to cause failure of the column or beam outside the connection. A beam section with a large plastic modulus was required; however, this plastic modulus had to be realized in the thickness of the flanges rather than in the depth of the beam. An increase of the beam depth would increase the strength of the connection region proportionally, so that the danger of a failure outside the connection is not diminished. Therefore, of beams with equal depths, only those with the greatest thickness of the flanges had been considered. Unless the beams and columns were designed in this way, a shear failure within the connection would not occur. Further, by omitting the required shear stiffening, the objective of obtaining a connection shear failure should be realized.

A second consideration was that the column and beam sections should form a connection of a realistic size and shape—that is, the beam depth should be greater than the column depth and the plastic moment of the beam should be approximately twice that of the column.

Interaction curves for combinations of sections were used to finally select an assemblage consisting of a W14 × 184 column and a W24 × 160 beam of ASTM-A36 steel.¹³ The interaction curves for the assemblage are shown in Fig. 7. This is a plot of the non-dimensional column force ratio P/P_y and the column moment M_a defined in Fig. 3 and non-dimensionalized by the full plastic moment of the column. These curves are dependent upon geometry and boundary conditions. The assumption was made that the column ends would be fixed against rotation. The beam section failure curve represents the value of M_a when a plastic hinge would form at the end of the beam. The column failure curve shown is Formula (2.4—3) of the AISC specification¹ for columns bent in double curvature. The other three interaction curves refer to general yielding of the connection using eq (4), (5), and (11) and equations of statics to relate beam moment to column moment M_a . At high axial load the interaction curves for the connection and the column outside the connection are very close. Obviously, the margin between connection yield from eq (11) and member failure outside the joint is a maximum when $P/P_y = 0.5$.

The geometry of the specimens of the previous test series⁴, called the A-series, was adopted in this test as shown in Fig. 6. That geometry was satisfactory except for the following points:

1. Local buckling occurred in both the beams and the columns.
2. The length of the column was too short. As a result, the shear force in the column was high and cancelled out a

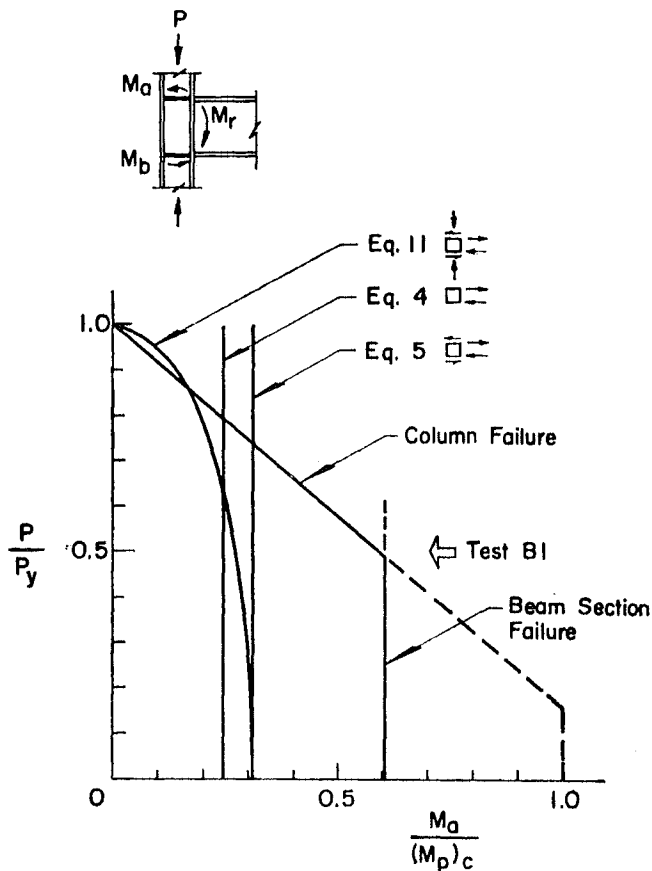


Fig. 7—Interaction curves for the assemblage consisting of W14×184 (column) and W24×160 (beam)

large part of the shear force in the connection.

These two factors caused failures in the A-series specimens outside the connection. The AISC design formulas¹ have been used to check for local buckling in this test. It was expected that the shear force in the column would be reduced sufficiently by taking a length of the column between inflection points of ten feet.

The length of the beam in Fig. 6 was determined by the capacity and stroke of the available hydraulic jacks, the available difference between the axial loads in the top and bottom parts of the column. As shown in Fig. 3, the axial load in the bottom part of the column was $P + V_r$ where V_r was the beam load. The objective here was to keep $P + V_r$ approximately equal to P to avoid premature column failure due to excessive reduction of M_{pc} at the section below the connection.

The details of the connection between the beam and column and the stiffening are shown in Fig. 8. Although the fabrication was completely done in the shop, the details are those of a welded field connection. An erection plate was fillet welded to the column flange. This plate had holes for erection bolts and was to be used as the backing strip for the beam web groove weld. The beam flange to column flange

welds were single bevel groove welds with $\frac{1}{4}$ in. root opening.

The horizontal stiffeners on the column web were designed according to the AISC specification¹ to resist the column web crippling force from the beam flange. The $\frac{5}{16}$ in. fillet welds connecting the stiffeners to the column flanges were the minimum allowed by the thickness of the parts joined.¹ However, these welds tore during the test (see Appendix) and were built up to $\frac{3}{4}$ in. fillet welds for completion of the test.

Section a-a in Fig. 8 shows that the stiffener was narrower than the beam flange width. There are no design guides concerning this detail, and the width of stiffener was governed by the limiting width-thickness ratio.¹

Test Setup

A special arrangement was devised to apply loads to the assemblage of Fig. 6. This setup is shown in Fig. 9. The axial load in the column was applied by a 5,000,000 lb capacity hydraulic universal testing machine. The crosshead of the testing machine through which the applied column load was measured is indicated. The base of the assemblage was bolted to the floor with four $1\frac{1}{2}$ in. bolts.

The beam load was applied through three 100,000 lb capacity hydraulic jacks in tension as shown in Fig. 10.

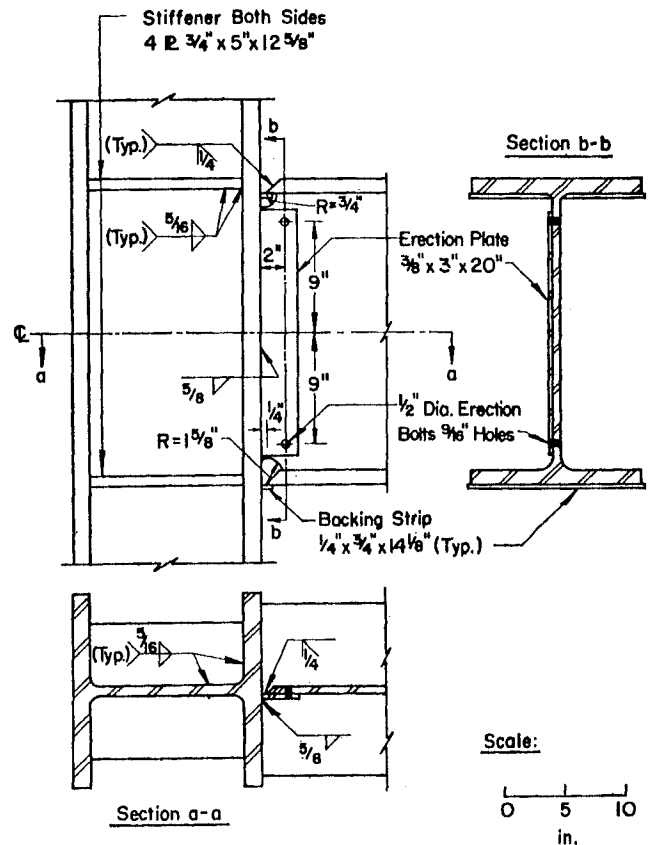


Fig. 8—Connection panel details

These jacks were arranged in a plane perpendicular to the plane of the assemblage, the center jack being vertical and the outside jacks being slanted away from the beam toward the floor. This loading scheme provided stability against lateral-torsional buckling of the cantilever beam.

The column ends were made flat-ended. This provided greater stiffness to the assemblage so that jack stroke would be conserved; however, the structure was more indeterminate as a result. The observed column end rotations are indicated in Fig. 11. The bending moment M_U in Fig. 3 could be applied to the testing machine crosshead with no distress to the system; however, the upper column shear V_a would cause the crosshead to drag on its guide rails. This condition was eliminated by providing a W36 × 194 beam to accept the column shear (see Fig. 9). The beam was connected to the column top plate through thirty $1\frac{1}{4}$ in. A325 high-strength bolts, and rested on its side, supported by two smaller members. The smaller members were bolted to the testing machine columns, and the stiff beam reactions were delivered to the sides of the testing machine through special bearing pads of mild steel. No lateral bracing was provided for the column.

In many respects this investigation was a pilot test to determine the feasibility of testing such assemblages under

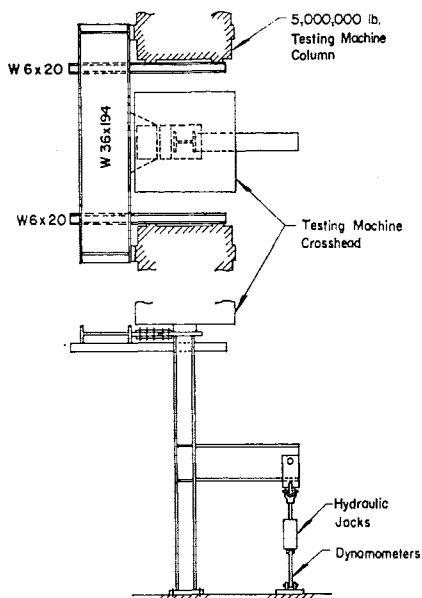


Fig. 9—Test setup

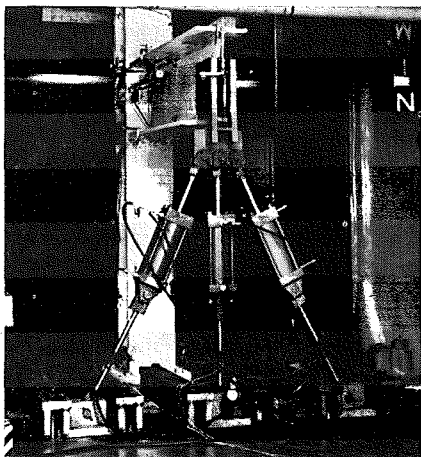


Fig. 10—Beam load applied by three hydraulic jacks

antisymmetrical loading condition. The setup was designed for reuse and has the following limiting conditions:

1. Maximum column load: 5,000,000 lb (Load tested to 819,000 lb)
2. Maximum beam load: 270,000 lb (Load tested to 216,000 lb)
3. Maximum stroke at end of beam: 11½ in. (Tested to 11½ in.)
4. Maximum column dimensions: 15¼ in. × 15¼ in. (Limitation is due to floor bolt hole pattern.)

Instrumentation

Strain gages and dial deflection gages were used to check forces and displacements. Four strain gages were located at each of four column cross sections as indicated in Fig. 12 Section a-a. These gages provided sufficient information to enable computation of the resultant axial force, bending moment, and shear in the column above and below the connection. The beam load was monitored by two strain

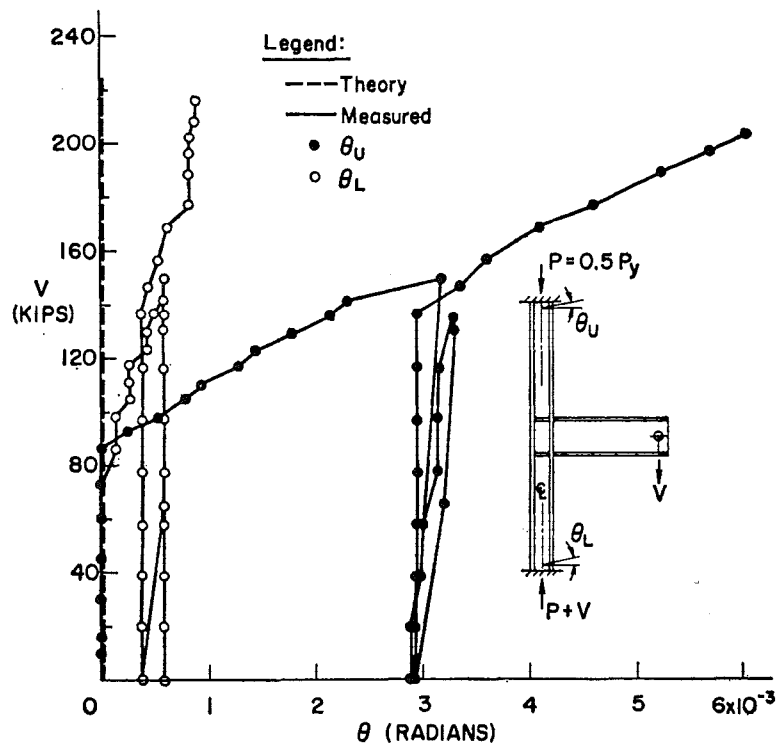


Fig. 11—Column end rotations

gages on the beam web, Section b-b. Stiffener strains were measured using four gages on each stiffener and one gage on the beam flange just outside the connection and directly in line with the stiffener gages. These strain gage locations are indicated in Fig. 12 Section c-c. Strains were automatically read and recorded.

Dial gages were employed to measure over-all column shortening, beam deflection, and lateral movement of the column midpoint. The arrangement of eight dial gages in the panel zone is shown in Fig. 13. This pattern was duplicated on the opposite side of the specimen so that measurements could be averaged, thereby excluding out of plane behavior.

Each dial gage was mounted on a post which in turn was tack welded normal to the column web. A wire was then stretched between the dial gage post and another post. The gage length, the distance between the two posts before straining, was recorded prior to the test. Two of the dial gages were used to measure diagonal deformation of the panel zone, one gage being mounted along each of the tension and compression diagonals. The other six gages were used to measure relative movement between the sections indicated in Fig. 12.

Translation and rotation was measured between sections c-c and d-d, d-d and e-e, and f-f and g-g. Sections d-d and f-f are the centerlines of the connection. Sections c-c and e-e were located 1 in. outside the connection boundaries. Section g-g was 4 in. away from the column flange.

The absolute rotations of both the top and bottom end plates of the column and of the support end of the beam were measured with level bars attached to the member webs directly inside the flanges. The locations of the level bars are indicated in Fig. 12.

The column load was applied and measured through the hydraulic universal testing machine. The beam load was measured using three dynamometers located in series with the hydraulic jacks in Fig. 10. The dynamometers were each calibrated before the test.

Before testing, the assemblage was whitewashed so that yielding patterns could be observed and photographed.

Mechanical Properties

Over-all dimensions of the assemblage as well as cross-sectional dimensions of the beam and column were measured. The over-all dimensions agreed with those in Fig. 6 to within 1/16 in. so those dimensions are not tabulated. The measured cross-sectional dimensions of the beam and column sections are given in Table 1 along with the corresponding dimensions from the AISC Manual.¹

Tensile tests were performed on specimens taken from the beam and column flanges and webs. Two specimens were cut from the flanges and two from the webs of each section. The test results in Table 2 are the static yield stress, the tensile strength, and the percent elongation in 8 in. Test results reported for the web are the average of two tests. The static yield stress is

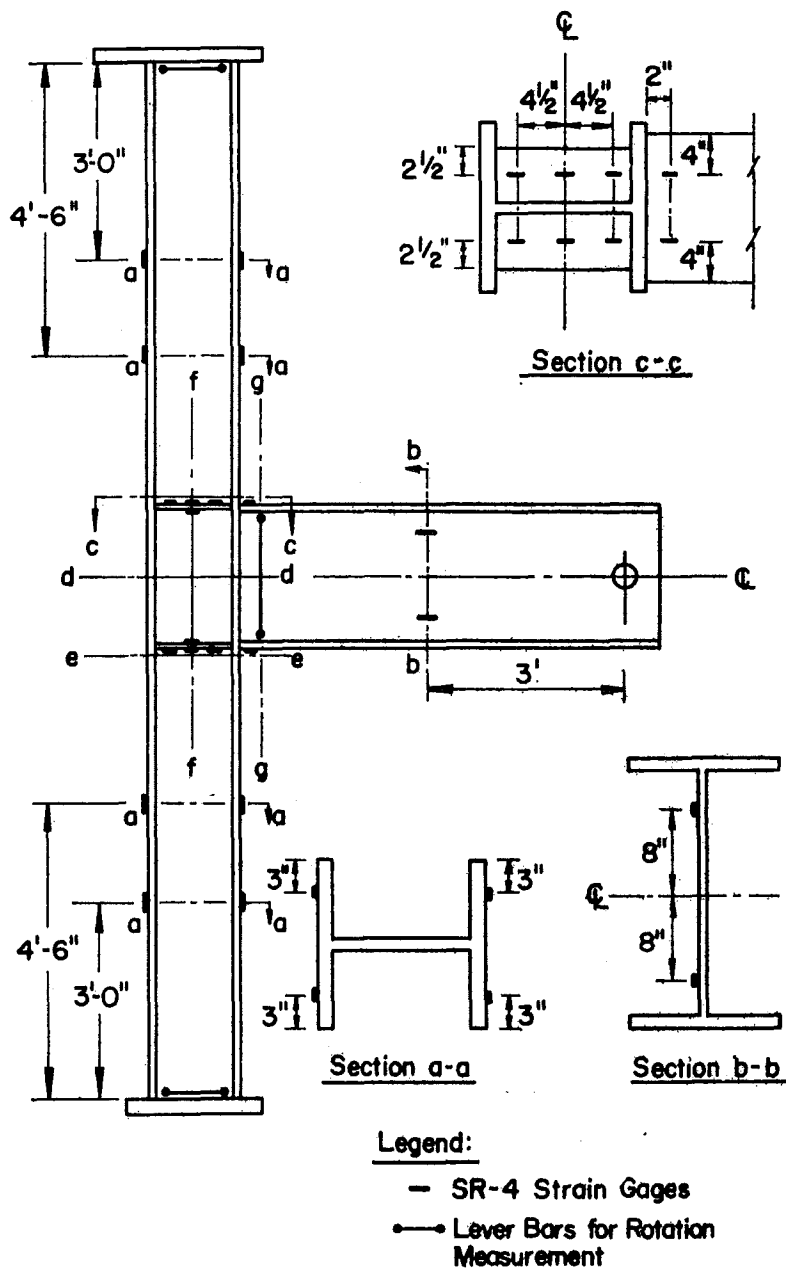


Fig. 12—Instrumentation

determined by reducing the testing speed to zero in the plastic region of the stress-strain relationship¹⁴. This procedure eliminates the effect of strain rate in the plastic region.

The mechanical properties from the mill report for the W14 × 184 are given on the bottom line of Table 2. The notable difference in yield strength is more than one might expect as a result of the difference in testing speed.

The yield stress from the web tests was used to compute V_1 , V_2 , and V_y' . P_y was calculated as the sum of the products of web area and web yield stress and flange area and flange yield stress.

Test Procedure

The testing sequence was as follows:
1. Column alignment.

2. Column loading up to 819 kips ($P/P_y = 0.5$).

3. Tightening transverse shear-pick up beam at top of column.

4. Beam loading to failure.

The column was considered to be aligned when the strain gages measuring axial strains in the column were in agreement within 10% at a column load of 100 kips. During the second step (column loading) a close watch was kept on the axial strains to ensure that the column was in fact receiving only an axial load. The column load of 819 kips was applied in five increments. At the end of each increment all instruments were read.

After the column loading was completed, the cross beam in Fig. 9 was tightened in place. This was delayed until after the column loading to pre-

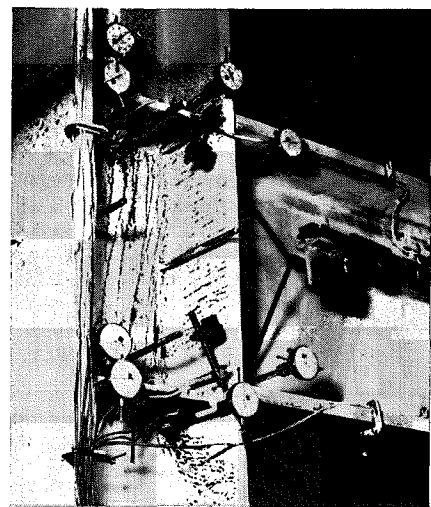


Fig. 13—Panel zone deformation measured by dial gages ($V = 117$ kips)

vent any sharing of the column load by the cross beam. After this precaution was taken, the beam loading was begun in 10 kip increments. During the entire beam loading phase the column load was maintained at 819 kips. Before instruments were read, all readings were permitted to stabilize under constant load; this required between ten and fifteen minutes for each increment of load.

Frequent visual inspections of the specimen and setup were made. As an added precaution, a transit was used to determine any possible lateral movement at the free end of the cantilever beam.

Test Results And Discussion

Column Shortening

The response of the column, as it was loaded to $0.5 P_y$, was in good agreement with elastic theory as indicated in Fig. 14. The abscissa is the column shortening as measured by a dial gage. The ordinates are, first, the column load P and then the beam load V . The column shortening increased elastically due to beam load until V_y' , the load that causes connection yielding, was reached. (V_y' is the beam load corresponding to the condition expressed by eq (15) and by eq (11) plotted in Fig. 7.) Beyond the load V_y' , inelastic column shortening was observed.

Beam Load and Deflection

Figure 15 shows the response of the assemblage in terms of the deflection Δ at the end of the cantilever beam. Deviation from elastic behavior was noted at 86 kips. The three reference loads V_1 , V_2 , and V_y' indicated on Fig. 15 were computed by solving eqs (4), (5), and (11) respectively for the assemblage. In eq (4):

$$M = V_1 \ell \quad (21)$$

Table 1—Specimen Dimensions (In.)

Element	Member	Beam		Column	
		W24 × 160		W14 × 184	
		AISC manual	Measured	AISC manual	Measured
Top ^a flange	Width	14.091	14.069	15.660	15.782
	Thickness	1.135	1.128	1.378	1.369
Web thickness		0.656	0.676	0.840	0.890
Bottom flange	Width	14.091	14.131	15.660	15.805
	Thickness	1.135	1.135	1.378	1.389
Depth		24.72	24.75	15.38	15.49

^a Top flange of column is on the beam side.

Table 2—Measured Mechanical Properties From Tensile Tests

Element	Member	Beam			Column		
		W24 × 160			W14 × 184		
		σ_y , ksi	σ_u , ksi	Elongation % in 8 in.	σ_y , ksi	σ_u , ksi	Elongation % in 8 in.
Top flange ^a		28.9	57.3	35.3	29.9	66.4	31.2
Web		33.3	62.4	31.7	31.4	63.9	32.2
Bottom flange		30.2	57.5	36.6	28.8	65.2	30.1
Mill report		—	—	—	45.1	67.7	26.2

^a Top flange of column is on the beam side.

where ℓ is indicated on the sketch in Fig. 15. In eq (5):

$$M_r = V_2 \ell \quad (22a)$$

$$M_l = 0 \quad (22b)$$

$$V_a = \frac{3}{2} V_2 \frac{L}{h} \quad (22c)$$

where L and h were defined in Fig. 3. In eq (11):

$$M_r = V_y' \ell \quad (23a)$$

$$M_l = 0 \quad (23b)$$

$$V_a = \frac{3}{2} V_y' \frac{L}{h} \quad (23c)$$

The member depths d_b and d_c have been taken as the distances between flange centroids ($d_b - t_b$ and $d_c - t_c$).² The condition that was assumed to obtain eqs (22c) and (23c) was that the column ends were fixed.

There is very little difference among V_1 , V_2 , and V_y' for the specific axial load $P/P_y = 0.5$ applied in this test. From Fig. 7 it is clear that V_2 calculated from eq (5) is equal to V_y' from eq (11) when $P = 0$. When the beam load exceeded the value V_y' , inelastic behavior was observed.

The basis for eq (4) (V_1), upon which the provisions of Part 2 of the AISC Specification rest, is a limit condition

of full yield. It is evident from this test under substantial axial load that this basis is conservative and that there is a considerable reserve of strength. This reserve is due first to the strength of the flanges and stiffeners that surround the web panel and act as a rigid frame. Second, it is due to subsequent strain-hardening of the connection web panel.

If the connection web had not yielded in shear, the simplified plastic theory could be used to predict a failure mechanism at the load V_{pc} .² The positions of plastic hinges for such a mechanism are indicated on the sketch in Fig. 15. Three hinges are required for a fixed-end column. The third hinge at the column base is not required if the ends are pinned. A second mechanism is possible: the formation of a single plastic hinge at the end of the beam. The predicted load levels at which each of these mechanisms would form are indicated in Fig. 15 by V_{pc} and V_p , respectively. The dashed lines in Fig. 15 represent the elastic-perfectly plastic behavior of the assemblage, the initial slope taking into account elastic shear deformation within the connection zone.

In the analysis it was assumed that no movement along the longitudinal axis of the beam was possible. This condition was only approximately achieved as shown by the data in Fig. 16. The maximum lateral movement at the beam level of the assemblage was 0.2 in. After the formation of three yielded zones the lateral deflection reversed in direction as would be expected for the mechanism indicated in the upper part of Fig. 16.

As the beam load V increased to 16 kips, flaking of the whitewash on the specimen in the connection panel was

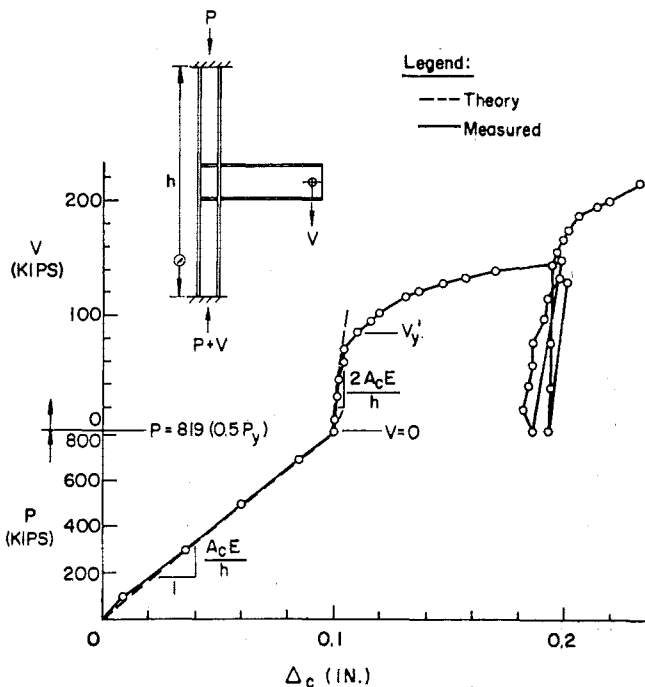


Fig. 14—Column shortening measured by over-all dial gage

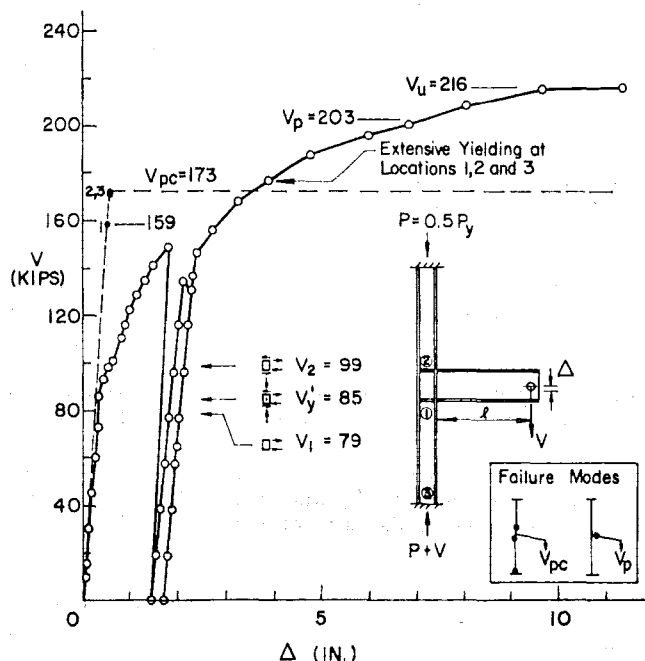


Fig. 15—Load-deflection curve of the connection assemblage—B1

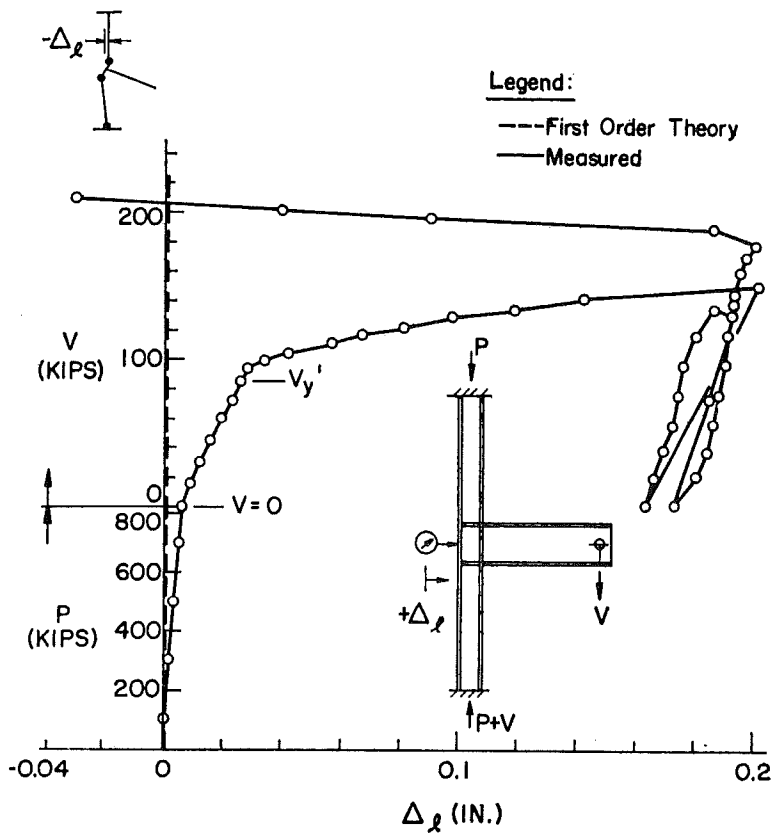


Fig. 16—Column lateral deflection

noticed. At 46 kips flaking of white-wash was observed on the exterior column flange along a horizontal band directly behind the top pair of horizontal stiffeners. This yielding raises some doubt concerning the validity of the flange bending model used to estimate the post-yield stiffness. At 86 kips excessive flaking in the connection panel was observed. At the same load Fig. 15 shows a definite decrease of stiffness. The appearance of the panel zone is shown in Figs. 13 and 17 at $V = 117$ kips.

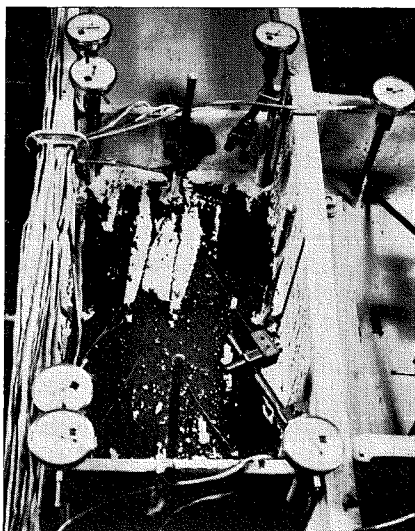


Fig. 18—Panel zone before repair of stiffener cracks ($V = 149$ kips)

Loading continued to 149 kips. At this point cracks were observed at the ends of the top horizontal stiffeners directly behind the beam tension-flange. These cracks occurred at the toes of the fillet welds. A later check of the design showed that these welds had been undersized. The original design of the fillet welds did not permit development of the full yield strength of the stiffener plates.

The specimen was unloaded and these fillet welds were burned out to the bottom of the cracks and replaced with larger welds that could develop the yield strength of the stiffener plates (see Appendix) although this may have been an overly conservative procedure. After the repair, there was no further difficulty with the stiffeners. The appearance of the panel zone and assemblage is shown in Figs. 18 and 19.

The assemblage was reloaded to 136 kips at which point the beveled groove weld of the top beam flange-to-column flange cracked. This crack was repaired by burning and rewelding (Appendix) but ultrasonic testing showed lack of fusion between the repair weld and base metal. A second repair of this crack was shown to be sound by ultrasonic testing and again the assemblage was reloaded. Extensive yielding began at the three locations indicated in Fig. 15 at 176 kips. Finally at 216 kips the maximum jack stroke was reached. Deflections increased at constant load until the jack stroke was depleted. At

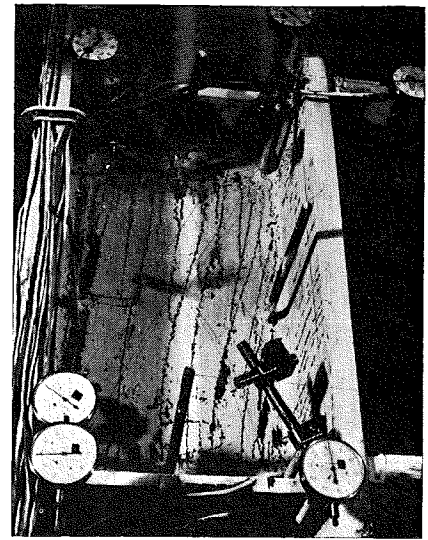


Fig. 17—Panel zone at $V = 117$ kips

this time photographs were taken of the yielding at the plastic hinge locations. Figure 20 shows this yielding above and below the connection and Fig. 21 shows the plastic region above the base plate.

The beam compression flange in Fig. 22 shows yielding and possible incipient local buckling. The beam moment exceeded the theoretical plastic moment for the $W24 \times 160$ by 6%. Figure 23 shows the permanent plastic deformation of the assemblage. The total amount of beam deflection of 11.5 in. was limited by the maximum jack stroke.

Although considerable deformation in the connection panel was observed toward the end of the test and despite its yielded condition, the panel was able to transmit the moments and forces applied to it. The tendency of axial load to accelerate the onset of yielding was observed.

Connection Shear Deformation

The connection panel shear stress was computed using eq (13). The column shear forces needed in that equation were computed from the moment

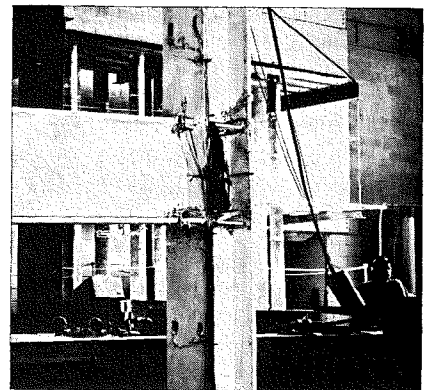


Fig. 19—Over-all view of connection assemblage B1 before repair of stiffener cracks ($V = 149$ kips)

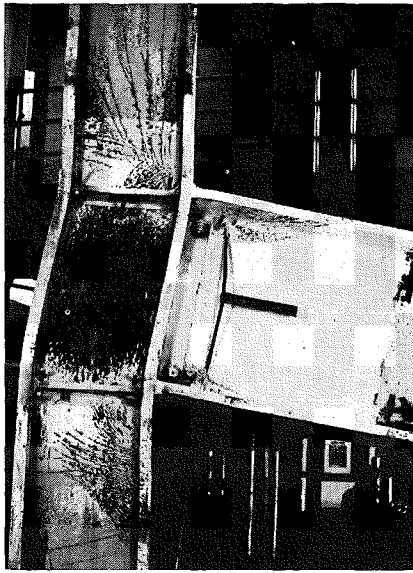


Fig. 20—Plastic regions below and above connection panel zone ($V = 216$ kips)

gradients given by strain gage measurements. Shear deformation was obtained by measuring the extension and contraction of the diagonals of the panel zone. The extension δ_7 and the contraction δ_8 are averaged to eliminate the components due to column axial load. This average deformation is directly proportional to the connection shear strain. The proportionality is dependent upon the distances between the measurement points d_1 and d_2 in the sketch in Fig. 24:

$$\gamma = \left(\frac{\sqrt{d_1^2 + d_2^2}}{d_1 d_2} \right) \delta \quad (24)$$

where

$$\delta = \frac{|\delta_7| + |\delta_8|}{2} \quad (25)$$

The shear stress-strain curve so obtained is plotted in Fig. 24. It should be remembered that this is not a shear stress-strain curve for a pure shear condition but rather for high shear in the web of a particular wide-flange section, the W14 \times 184. The elastic region of this curve agrees well with the elastic shear stress-strain curve using the elastic shear modulus $G = 11,500$ ksi. The inelastic region predicted by eqs (13) and (20):

$$\frac{\tau}{\gamma} = \frac{Q}{A_w \gamma} = \frac{24 EI_f}{A_w d_b^2} \quad (26)$$

is dependent upon the elastic properties of the web boundary.

The stresses τ_y and τ_y' in Fig. 24 are obtained from eq (10) assuming $P = 0$ and $P = 0.5 P_y$ respectively. The stress τ_y' more accurately defines the experimentally observed yield stress. The post yield stiffness is predicted by accounting for the flange-stiffener boundary strength.



Fig. 21—Plastic region above base plate ($V = 216$ kips)

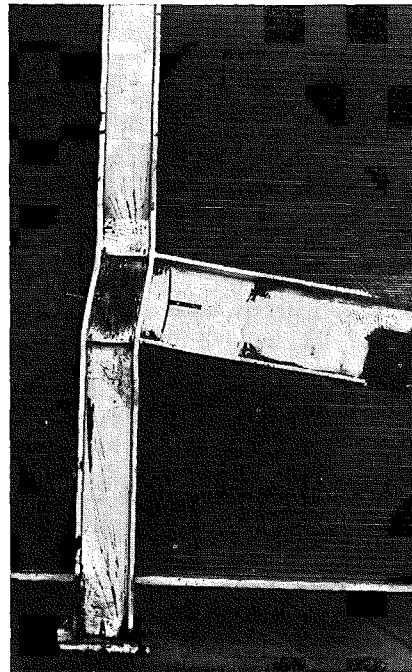


Fig. 23—Over-all view of connection assemblage B1 after testing

Connection Compression

The column shortening indicated in Fig. 14 agreed with theory until the beam load exceeded V_y' at which the connection yielded. After V_y' , the column outside the connection was still unyielded so the shortening should not be ascribed to those parts of the column. Furthermore, the column load above the connection remained constant and below the connection increased only slightly so that further elastic column shortening was small. The connection panel compression, then, must be an allied effect to the joint shear deformation γ . The relationship between the connection shortening Δ_j and γ is indicated in the sketch in Fig. 25:

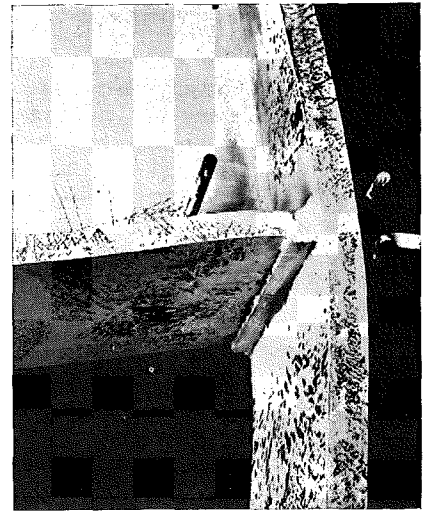


Fig. 22—Local buckling of beam compression flange ($V = 216$ kips)

$$\Delta_j = d_3 (1 - \cos \gamma) \quad (27)$$

where d_3 is the distance between measurement pins. Using the first two terms of an infinite series for $\cos \gamma$ gives:

$$\Delta_j = d_3 \left(\frac{\gamma^2}{2} \right) \quad (28)$$

This relationship has been graphed in the upper portion of Fig. 25 and so have the experimental results from dial gage measurements of Δ_j . The shear strain values used in eq (28) were the measured values indicated in Fig. 24. Evidently, the second order effect of large shear strains expressed by eq (28) can become quite substantial.

Beam Support End Rotation

The rotation at the connection end of the cantilever beam plotted in Fig. 26 indicates the large rotations that are encountered after the connection panel yields. The rotation θ_b is absolute rotation measured with a level bar. The theoretical curve was calculated assuming a fixed-end column taking into account elastic shear deformation within the connection zone. After $V_y' = 85$ kips, a second theoretical slope, calculated using the connection stiffness expressed by eq (20), is shown. The indication here is that the approximations used in eq 20 are acceptable for loads in excess of V_y' and that the rotation θ_b becomes larger than the predicted value as yielding becomes extensive in the connection.

Stiffener Strains

Strain gages were mounted on all horizontal stiffeners. The two plots in Fig. 27 show the variation of strain along a compression stiffener and a tension stiffener. The locations of the strain gages are indicated below the plots. The stiffener strains are indicated for four different beam loads V . Above

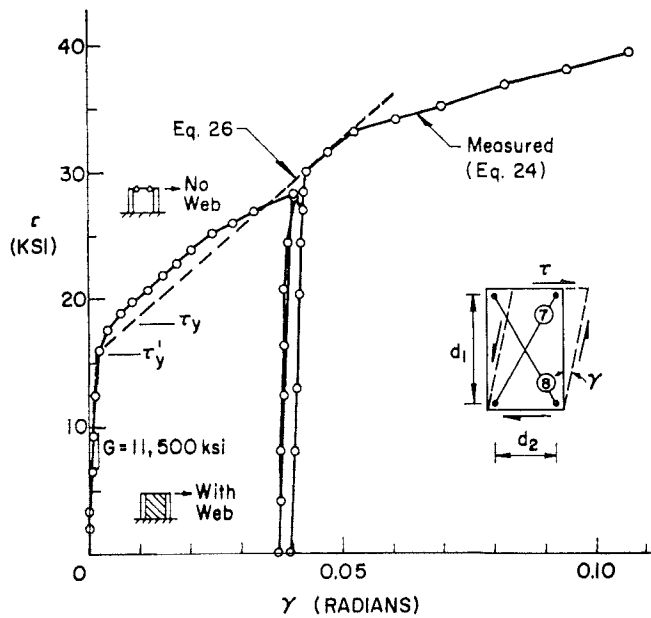


Fig. 24—Panel zone shear stress versus shear strain determined by diagonal gages 7 and 8

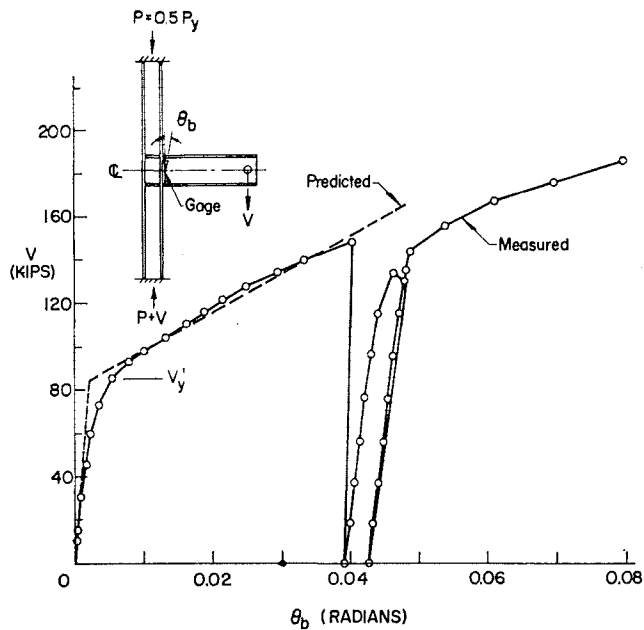


Fig. 26—Beam load versus beam support end rotation

Fig. 27 (right)—Stiffener strains

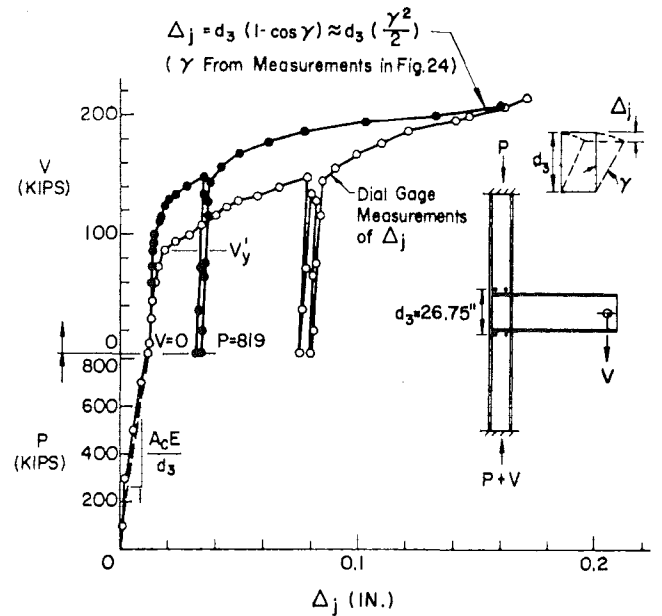
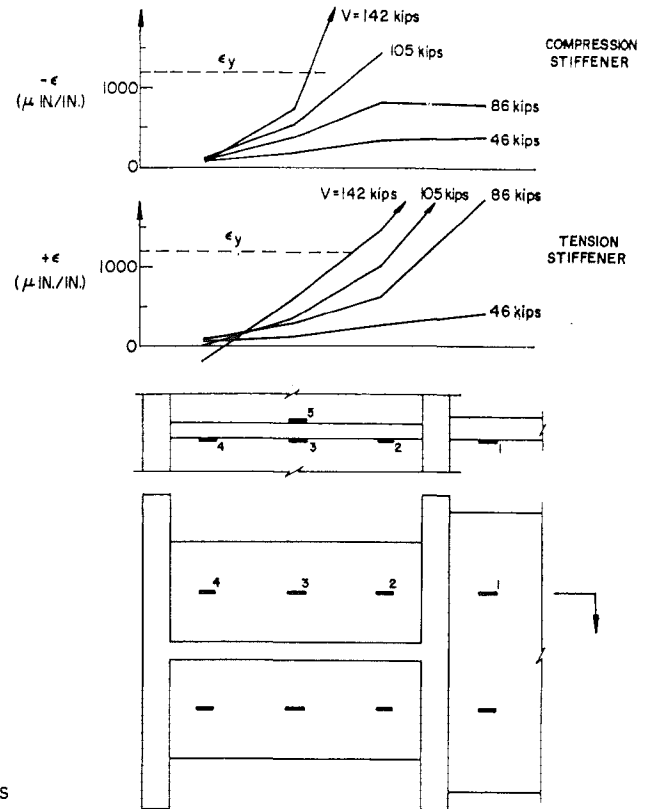


Fig. 25—Column and beam loads versus connection shortening



$V = 86$ kips the strains measured in the beam flanges at location 1 became extremely large. This was due to the proximity of the gage and the beam groove weld, an area of high residual stress and a certain degree of stress concentration.

The strains in the stiffeners decreased from a maximum at the beam connection end to zero at the other end. This would seem to indicate that the stiffener force is transferred to the web within its length and that welds are not needed where the stiffener joins the

exterior column flange. Such a possibility must be more fully studied.

Strains exceeded the yield strain ($\epsilon_y = 1200 \mu \text{ in./in.}$) at location 2 in the compression stiffener for $V = 105$ kips and in the tension stiffener for $V = 142$ kips. This indicates that the stiffeners developed their full yield strength. Furthermore, because the strains decreased to zero along the stiffener, the transfer of the full yield strength of the stiffener to the column web was effected.


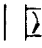
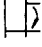

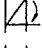
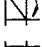
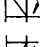
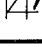
These results suggest that the stiffener welds be sized to transmit a force

equivalent to the yield load of the stiffener plate.

Maximum Load

A defined ultimate load for the connection was not observed. The observed maximum load V_u at 216 kips was limited by jack stroke; however, a sufficient number of yielded zones had formed to permit the structure to deform plastically without further increase in load. The predicted ultimate load V_{pc} from simplified plastic theory was 173 kips. The difference between V_u and V_{pc}

Table 3—Tests Results of B1 And A Series^a

Test	Column size	P P _y	Experimental		Reference		V _u V _{pc}	V _o V _y '	V ₂	V _u V _{pc}	V _o V _y '	V _o V ₂
			V _u	V _o	V _{pc}	V _y '						
	B1	W14 × 184	0.50	216.0	86	173.0	85.0	99.0	1.25	1.01	0.87	
	A1	W6 × 25	0.60	39.2	26	30.4	25.1	31.4	1.29	1.03	0.82	
	A2	W6 × 25	0.80	35.6	22	12.9	18.9	31.5	2.76	1.16	0.70	
	A3	W6 × 20	0.60	29.1	23	17.5	—	—	1.66	—	—	
	A4	W6 × 20	0.80	22.8	15	10.2	—	—	2.23	—	—	
	A5	W6 × 20	0.80	17.4	13	13.3	—	—	1.31	—	—	
	A6	W6 × 20	0.60	27.1	22	19.5	—	—	1.39	—	—	
	A7	W6 × 25	0.80	35.0	20	12.7	—	—	2.75	—	—	

^a All beam sections of A series are M12 × 16.5; all loads listed are beam loads (V) in kips.

is evidently due to strain-hardening in the plastic zones outside the connection. This effect has been explained in previous work.¹¹

The onset of inelastic behavior at $V_{y'}$ was clearly observed. The inelastic column web deformation was predicted by theory in the range of plastic deformations.

A table containing the experimental and reference loads discussed above is given as Table 3. The first row of this list contains the data for the test reported herein, Specimen B1. The tests designated A1 to A7 were reported by Peters and Driscoll.⁴ A sketch of the joint detail is given in the column to the left of the specimen designation. The column sizes are given for the assemblages all of which were similar to that in Fig. 3. Axial load ratios P/P_y are listed for the column segment having the smaller axial load. (Refer to Fig. 3.)

The experimental ultimate loads V_u and the observed yield loads V_o are given next. V_o is taken as the load at which deformations deviate from an elastic prediction. The reference load V_{pc} is the predicted ultimate load computed using the mechanism method of the simplified plastic theory.² $V_{y'}$ and V_2 are calculated from the equations presented previously.

The ratio V_u/V_{pc} shows the reserve strength of the assemblages over the prediction from simplified plastic theory. For connections with no shear stiffening A1, A2, and B1 there was no reduction in ultimate load. The final columns in Table 3 are the ratios of the observed yield load to the calculated yield loads $V_o/V_{y'}$ and V_o/V_2 . These ratios are listed only for connections with no shear stiffening with $V_{y'}$ considering axial load. The data indicate that the equations for $V_{y'}$ can be used to predict connection yielding due to shear and axial load.

The above predictions of connection behavior have been achieved without considering strain-hardening. This means that connection web deformation follows elastic-perfectly plastic behavior fairly well rather than to lead to immediate strain-hardening. To utilize this knowledge in design (through permitting higher allowable shear in webs) will require evaluation of the effect of the deformations on frame behavior. If the consequences of connection deformation are tolerable, then no connection shear stiffening is necessary. In addition, where stiffening is required the amount of such stiffening must be based on the required connection rigidity rather than on the criterion defining connection yielding—eq (11)—since post yield stiffness has been demonstrated.

Conclusions

1. Yielding of the connection was predicted with accuracy using the Von Mises yield criterion to account for the axial load effect—eq (11).
2. The ultimate load of the assemblage occurred after the formation of yielded zones outside the connection—Fig. 15.
3. Column web deformations within the connection can be predicted satisfactorily in the elastic range and the initial portion of the inelastic range—Fig. 24.
4. There was a large margin of reserve strength in the connection that should be considered in design. The strength of the assemblage exceeded all theoretical ultimate loads—Table 3.
5. Any revision of connection shear stiffening requirements must be based on required rigidity because shear capacity exceeds that given by the yield criterion—eq (11).
6. The horizontal stiffeners, designed

according to the 1969 AISC Specification, behaved satisfactorily.

7. Weld detail and quality were shown again to be important factors in joint design. Welds approved by ultrasonic tests were satisfactory.

Acknowledgements

This work was sponsored by the American Iron and Steel Institute and the Welding Research Council. The authors are grateful for their financial support and the technical assistance provided by the WRC Task Group, of which J. A. Gilligan is Chairman.

The project under which this report was written is directed by Dr. L. S. Beedle with Dr. G. C. Driscoll, Jr. and Dr. W. F. Chen as advisors. The work was carried out at the Fritz Engineering Laboratory, Department of Civil Engineering, Lehigh University. Dr. L. S. Beedle is Director of the Laboratory and Dr. D. A. VanHorn is Chairman of the Department.

The authors are especially thankful to Messrs. J. A. Gilligan, C. F. Diefenderfer, and C. L. Kreidler for their particular assistance in the fabrication, testing, and inspection phases of this work. Messrs. I. J. Oppenheim and C. Bennett contributed their time to testing and reduction of data. Thanks are also due Mr. W. E. Edwards for his valuable comments on this report.

References

1. Manual of Steel Construction, Specification (and Commentary) For the Design, Fabrication, and Erection of Structural Steel For Buildings, 7th Edition, American Institute of Steel Construction, 1970.
2. Plastic Design in Steel, ASCE Manual 41, 2nd Edition, The Welding Research Council and The American Society of Civil Engineers, New York, 1971.
3. Yura, J. A., "The Strength of Braced Multi-Story Steel Frames", Fritz Laboratory Report 273.28, Lehigh University, Bethlehem, Pa. 1965.

4. Peters, J. W., and Driscoll, G. C., Jr., "A Study of the Behavior of Beam-To-Column Connections", Fritz Laboratory Report 333.2, Lehigh University, Bethlehem, Pa. 1968.

5. Naka, T., Kato, B., and Watabe, M., "Research On The Behavior of Steel Beam-To-Column Connections", Laboratory for Steel Structures, Dept. of Architecture, University of Tokyo, 1966.

6. Beedle, L. S., "Plastic Design of Steel Frames", John Wiley and Sons, Inc., New York, 1958.

7. Lyse, I., and Godfrey, H. J., "Investigation of Web Buckling in Steel Beams", Fritz Laboratory Report 155.1, Lehigh University, Bethlehem, Pa. 1933.

8. Beedle, L. S., Topractsoglou, A. A., and Johnston, B. G., "Connections for Welded Continuous Portal Frames", Progress Report No. 4, WELDING JOURNAL, 30 (7), Research Suppl., 359-s to 384-s (1951).

9. Seely, F. B., and Smith, J. O., "Advanced Mechanics of Materials", 2nd Edition, John Wiley and Sons, Inc., New York, 1932.

10. Ros, M., and Eichinger, A., "Experimental Investigation of Failure Theories (Versuche Zur Klaerung Der Frage Der Bruchgefahr), Diskussionsbericht Nr. 34, Eidgenoessische Materialpruefungsanstalt an Der E. T. H. in Zurich, 1929.

11. Lay, M. G., and Galambos, T. V., "Inelastic Steel Beams Under Moment Gradient", Journal ASCE, 93 (ST1), P. 381 (February 1967).

12. Van Zullen, L., Fielding, D. J., and Driscoll, G. C., Jr., "Proposal for Test of Full Size Beam-To-Column Connection Subjected to Moment, Shear, and High Axial Loads", Fritz Laboratory Report 333.4, Lehigh University, Bethlehem, Pa., 1968.

13. Standard Specification For Structural Steel, American Society for Testing and Materials, Philadelphia, 1967.

14. Beedle, L. S., and Tall, L., "Basic Column Strength", Journal ASCE, 86 (ST7), p. 139, (July, 1960).

Appendix

Nomenclature

A_c	Profile area of column
A_w	Area of column web
E	Modulus of elasticity of steel
G	Shear modulus of elasticity of steel
I_f	Moment of inertia of individual flanges of a beam or column
L	Distance between column centerline and load point in beam
M	Moment (kip-feet)
M_a	Moment above connection
M_b	Moment below connection
M_L	Moment in assemblage at floor base plate
M_l	Moment at the left-hand side of a connection

M_p	Plastic moment
M_{pc}	Plastic hinge moment modified to include the effect of axial compression
M_r	Moment at the right-hand side of a connection
M_U	Moment in assemblage at column top plate
P	Applied column load
P_a	Column load above connection
P_b	Column load below connection
P_l	Axial load in beam to the left of a connection
P_r	Axial load in beam to the right of a connection
P_y	Plastic axial load; equal to profile area times yield stress (kips)
Q	Shear force within a connection
Q_f	Portion of shear force within a connection carried by the column flanges
Q_u	Plastic connection shear force; equal to web area times shear yield stress (kips)
T	Force system statically equivalent to bending moment
V	Statical shear in any member; also beam load (kips)
V_u	Shear force above connection
V_b	Shear force below connection
V_l	Shear force in the member to the left of a connection
V_o	Beam load at observed yield
V_p	Beam load causing plastic hinge at support end of cantilever
V_{pc}	Beam load causing column mechanism
V_r	Shear force in the member to the right of a connection
V_u	Statical shear (or beam load) produced by "ultimate" load in plastic design (kips)
V_u'	Statical shear (or beam load) at connection yield according to Von Mises yield criterion
V_1	Statical shear (or beam load) at connection yield neglecting axial load and column shear effects
V_2	Statical shear (or beam load) at connection yield neglecting axial load effect
b_f	Flange width of rolled section
d_b	Depth of beam

d_c	Depth of column
d_1, d_2, d_3	Distances between deflection measurement pins
h	Assemblage column height between fixed ends
ℓ	Distance between cantilever beam support end and loading point
t_b	Beam flange thickness
t_c	Column flange thickness
t_f	Flange thickness, in general
w	Column web thickness
Δ	Deflection at free end of cantilever beam (in.)
Δ_c	Axial column deflection
Δ_j	Axial connection deflection
Δ_l	Deflection in the direction of the beam axis
γ	Shear strain (radians)
γ_u'	Shear strain at shear yield stress; τ_u'/G
δ	Diagonal connection deflection (in.)
δ_n	Dial gage deflection where "n" refers to a particular gage number
ϵ	Strains measured by SR-4 strain gages
θ_b	Absolute joint rotation (radians)
θ_L	Rotation of column base (radians)
θ_U	Rotation of column top (radians)
σ	Normal stress on an element (ksi)
σ_a	Normal stress along a-axis
σ_b	Normal stress along b-axis
σ_y	Static yield stress from tension test
σ_u	Ultimate tensile stress from tension test
τ	Shear stress on an element (ksi)
τ_{ab}	Shear stress on element in plane of axes "a" and "b"
τ_y	Shear yield stress in the absence of axial stress; $\sigma_y/\sqrt{3}$
τ_y'	Shear yield stress in the presence of axial stress

Repair of Connection Assemblage B1

1. Crack no. 1 caused by under-designed fillet weld—Fig. A. Crack burned out and fillet weld replaced

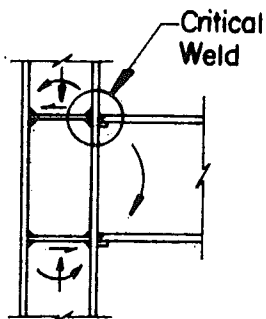


Fig. A

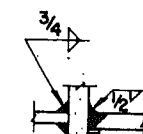
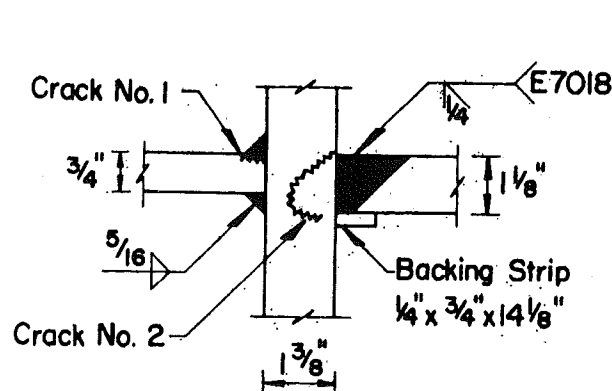


Fig. B

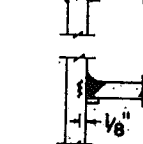


Fig. C



Fig. D

with $\frac{3}{4}$ in. fillet weld—Fig. B.

2. Crack no. 2 caused by stress concentration at intersection of flanges—Fig. A.

(a) Arc-air out to bottom of crack checking for bottom of crack by

magnafluxing.

(b) Reweld with E7018 electrodes. Add a contouring fillet weld ($\frac{1}{2}$ in. leg)—Fig. B.

(c) Ultrasonic inspection: Weld rejected due to lack of fusion as

indicated in Fig. C.

3. Crack no. 2 re-repaired by removing backing strip and burning out from bottom of flange—Fig. D. Reweld approved on the basis of ultrasonic inspection.